

# V2XP-ASG: Generating Adversarial Scenes for Vehicle-to-Everything Perception

Hao Xiang<sup>1\*</sup>, Runsheng Xu<sup>1\*</sup>, Xin Xia<sup>1</sup>, Zhaoliang Zheng<sup>1</sup>, Bolei Zhou<sup>1</sup>, Jiaqi Ma<sup>1†</sup>

**Abstract**—Recent advancements in Vehicle-to-Everything communication technology have enabled autonomous vehicles to share sensory information to obtain better perception performance. With the rapid growth of autonomous vehicles and intelligent infrastructure, the V2X perception systems will soon be deployed at scale, which raises a safety-critical question: *how can we evaluate and improve its performance under challenging traffic scenarios before the real-world deployment?* Collecting diverse large-scale real-world test scenes seems to be the most straightforward solution, but it is expensive and time-consuming, and the collections can only cover limited scenarios. To this end, we propose the first open adversarial scene generator V2XP-ASG that can produce realistic, challenging scenes for modern LiDAR-based multi-agent perception systems. V2XP-ASG learns to construct an adversarial collaboration graph and simultaneously perturb multiple agents’ poses in an adversarial and plausible manner. The experiments demonstrate that V2XP-ASG can effectively identify challenging scenes for a large range of V2X perception systems. Meanwhile, by training on the limited number of generated challenging scenes, the accuracy of V2X perception systems can be further improved by 12.3% on challenging and 4% on normal scenes. Our code will be released at <https://github.com/XHwind/V2XP-ASG>.

## I. INTRODUCTION

Over the past decade, we have witnessed tremendous progress in Autonomous Vehicles (AVs) [1], [2], [3], [4], [5], [6], [7], [8], [9], [10], [11], [12], [13], [14] and intelligent transportation systems [15], [16], [17]. Sooner, these autonomous systems will be deployed on roads at scale, opening up opportunities for cooperation between them. Previous works [18], [19], [20], [21], [22], [23] have demonstrated that by leveraging the Vehicle-to-Everything (V2X) communication technology, AVs and infrastructure can perform cooperative perception by using the shared sensing information and thus significantly enhance the perception performance [24], [25], [26], [27], [28]. Despite the remarkable improvement, these works evaluate the proposed systems on the dataset with natural scenarios that do not contain sufficient safety-critical scenes. Under the challenging scenes, these systems may have inferior performance, and thus it is crucial to identify challenging scenes to fully understand the robustness of existing cooperative perception systems. The straightforward solution is to collect a wide range of testing scenes in the real world and identify critical ones. However, compared to single-agent systems, the cost and time consumption of gathering and labeling data for multi-agent systems can be much more demanding. A preferable cost-effective solution

is to generate large-scale realistic scenes [29], [30], [31] in high-fidelity simulators. Yet these approaches only consider the common scenes and lack the capability of performing stress tests on corner cases for the target systems.

To address this problem, inspired by recent works [32], [33], [34] that produce safety-critical scenarios for the single-agent planner by perturbing surrounding vehicles’ trajectories, we aim to automatically generate diverse and challenging scenes for V2X perception systems. Nonetheless, it is demanding to directly transfer the single-agent scenario generation methods to V2X systems. Unlike the single-agent system with a single viewpoint, V2X system involves collaborators with multiple viewpoints. The geometric relationships between these views from distinct collaborators can vastly influence the perception performance [35], which is not considered in the previous works. Furthermore, the collaborator choices can influence the viewpoints and thus are coupled with the agent pose perturbations, leading to more complicated interactions. Handling these differences between single-agent and cooperative perception is the key to an effective V2X adversarial scene generator. However, no literature has been reported to investigate them. Moreover, most existing methods are tailored for planning, and there is no publicly available scene generation framework for perception, which hinders the progress of developing efficient scene generation methods for modern single-agent and V2X perception systems.

To this end, we introduce V2XP-ASG – the first open Adversarial Scene Generator for LiDAR-based V2X Perception systems. To the best of our knowledge, this is the first framework that aims to automatically generate challenging scenes for V2X perception. As shown in Figure 1, given an initial scene from the dataset, V2XP-ASG first constructs an adversarial collaboration graph by searching for adversarial collaborators whose viewpoints combination will lead to inferior performance. Afterward, we perturb multiple agents’ poses in an adversarial and plausible way. To reflect the updated LiDAR observation caused by sensor viewpoint change and pose perturbation, we conduct the experiments based on the high-fidelity CARLA [36] simulator. Extensive experiments show that V2XP-ASG can create challenging scenes to severely deteriorate the performance of modern V2X perception systems. More importantly, training with these adversarial scenes can increase the system’s accuracy. Our main contributions can be summarized as follows

- We present V2XP-ASG, the first open adversarial scene generation framework, to test modern V2X perception systems. Our V2XP-ASG can intelligently generate challenging scenarios for a wide range of V2X perception

\*Equal contribution.

<sup>1</sup> University of California, Los Angeles, CA, USA.

<sup>†</sup> Corresponding author: [jiaqima@ucla.edu](mailto:jiaqima@ucla.edu).

systems plausibly. We will release codes in the future.

- We formulate this scene generation task as a novel two-stage optimization problem, which makes the optimization easier and provides interpretability to the system’s weakness.
- We propose an efficient search strategy for the novel Adversarial Collaborator Search (ACS) task in the first stage by leveraging learnable collaboration graph weights. Moreover, in the second stage, we employ the black-box optimization algorithms with customized adversarial objectives for perception tasks to perturb vehicle poses in an adversarial and feasible manner. These two stages are combined to efficiently raise the scene’s challenging level.
- As demonstrated by our experiments, training on generated adversarial scenes can greatly improve the system’s precision under both normal and challenging scenes.

## II. RELATED WORK

**V2X Perception:** V2X perception investigates how to leverage the visual information from nearby AVs and intelligent infrastructure to enhance the perception capability. Based on the collaboration strategies, there are three major classes: early [37], late [38], [39], [40], and intermediate fusion [41], [42], [43], [44], [45], [46], [47], [48]. The early fusion method delivers the raw point clouds across agents, and each agent will feed the aggregated point clouds to the network for 3D detection. Despite preserving complete raw information, early fusion usually requires large bandwidth, making it unrealistic to deploy [49], [50]. On the contrary, late fusion has a minimum data transmission size as it only circulates the metadata of prediction outputs. However, its accuracy is limited since it fails to provide valuable scenario context [41]. To achieve a good trade-off between bandwidth and accuracy, intermediate fusion, which broadcasts the compressed intermediate neural features, has been mostly studied recently. [41] proposes a spatial-aware graph neural network for joint perception and prediction, and [44] employs knowledge distillation to advance the learning with the supervision of early fusion. [42] proposes a location-wise self-attention mechanism to fuse the features from different AVs. This work evaluates all three fusion strategies and the single-agent perception method.

**Adversarial Scenario Generation:** As safety is critical to autonomous driving [51], recently, several works [32], [33], [34], [52] have been proposed to generate safety-critical scenarios for identifying planning failures. [32] uses Bayes Optimization to search crash scenarios based on a hierarchical graph route in CARLA [36]. STRIVE [33] represents agents in latent space via a graph-based conditional VAE model and perturb latent variables via gradient-based optimization to produce trajectories that collide with a given planner. AdvSim [34] benchmarks several black-box optimization algorithms to search adversarial trajectories to obtain safety-critical scenarios for the full autonomy stack, but its adversarial objective is targeted for planning, and it is designed for the single vehicle system. Another stream of

work [53], [54] formulates the scenario generation problem as the rare event simulation to sample failure scenarios for the single-agent autonomy system. In contrast, we focus on producing challenging scenarios for the LiDAR-based multi-agent V2X perception system where both the agents’ poses and the selection of collaborators are searched to optimize an adversarial objective customized for perception.

**LiDAR-based adversarial attack:** LiDAR-based adversarial attacks [55], [56], [57] in a physically realizable way have gained increasing attention. [57] performs the first security study of LiDAR-based perception in AV settings by changing raw LiDAR points via a LiDAR spoofer. [56] studies the backdoor of motion compensation and performs adversarial spoofing of the agent’s trajectory to deteriorate the perception performance. In [55], an adversarial mesh is put on the rooftop of a vehicle, and mesh poses are optimized to make the vehicle invisible. Besides the above single-agent attack, [58] attacks the V2X perception system by adding adversarial noises to the intermediate features shared by intelligent agents. Different from previous work, we directly attack the agent collaboration choice and vehicle poses to deteriorate the performance of the modern V2X perception system, which ensures the feasibility and plausibility of the generated adversarial examples.

**Multi-agent collaboration graph:** A classical multi-agent collaboration graph focuses on fusing information from selected agents or all the connected agents to increase the system’s performance. Who2com [35] proposes a handshake communication mechanism where the neural network can learn and determine which two agents should compress relevant information needed for each stage. When2com [59] constructed learning-based communication groups to learn to communicate and used an asymmetric attention mechanism to decide when to communicate across a fully-connected graph. DiscoGraph [44] exploited a method that incorporates both early and intermediate collaboration into a knowledge distillation framework, which enables the knowledge of early collaboration to guide the training of an intermediate fusion model. However, rather than trying to improve the perception performance by finding robust collaborators, in this work, we are interested in searching for adversarial collaborators to deteriorate the task performance, which can help expose the potential vulnerability of the multi-agent system.

## III. ADVERSARIAL SCENE GENERATION

V2XP-ASG aims to generate realistic, challenging scenes for a given V2X perception model. The overall architecture of our framework is shown in Figure. 1, which consists of Adversarial Collaborator Search (ACS) and Adversarial Perturbation Search (APS). Given an existing scene with a fixed ego agent, we first search for adversarial collaborator combinations by leveraging an attention-based sampling approach and then build the adversarial collaboration graph with selected agents. Afterward, we perturb multiple agents’ poses and feed updated LiDAR observation into the target perception system to generate 3D bounding boxes. Eventually, we evaluate the predictions with adversarial objectives and perform black-box optimization to update poses.

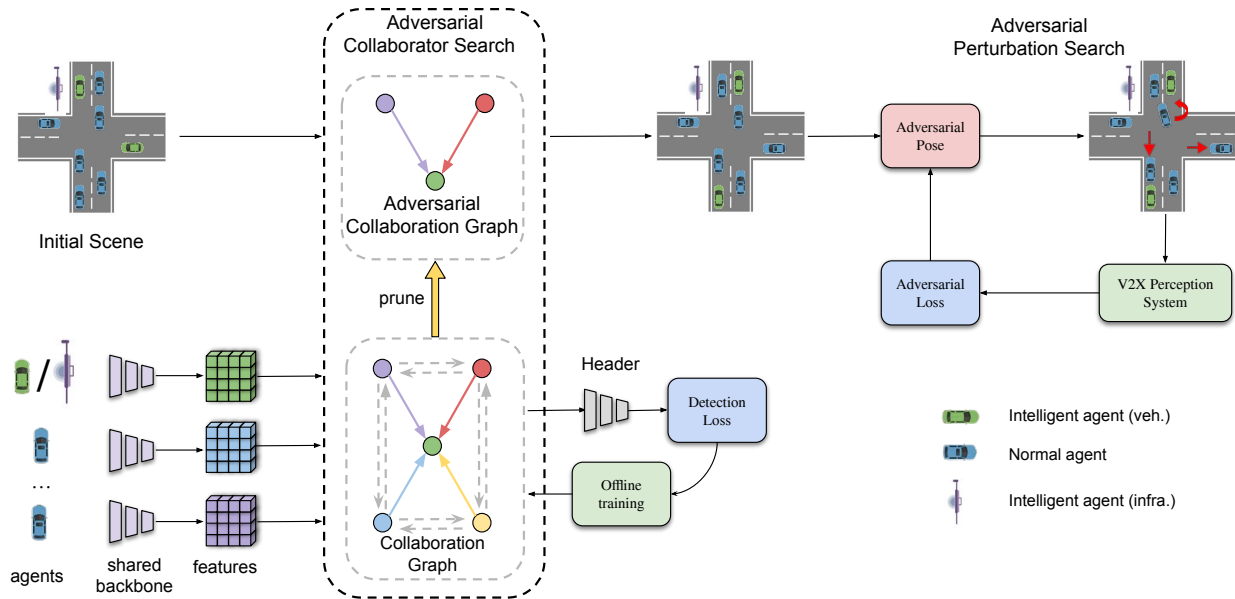


Fig. 1: **Overview of proposed V2XP-ASG.** It contains two steps: adversarial collaborator search and adversarial perturbation search. Details for each component can be found in Sec. III

### A. Problem formulation

Given an initial scene with a set of agents  $\mathcal{A} = \{a_1, \dots, a_N\}$  where agents  $a_i$  can be either vehicle or infrastructure, we assume  $k$  of them are equipped with sensing and communication devices and are denoted as intelligent agents  $\mathcal{I} \subset \mathcal{A}$ . Within the communication range, all the agents belonging to  $\mathcal{I}$  can share information with each other and one of them is selected as the ego agent to aggregate the sensing information to form a unified detection. More formally, the set of observations from these agents are

$$\mathcal{X}(\mathcal{S}, \mathcal{I}) = \{\mathbf{X}_i(\mathcal{S}) \mid \forall i \in \mathcal{I}\} \quad (1)$$

where  $\mathcal{S} = \{s_1, \dots, s_N\}$  is the set of poses of all agents in the scene.  $\mathbf{X}_i(\mathcal{S})$  is the sensing observation from intelligent agent  $i$  and it reflects the change of agents' poses  $\mathcal{S}$ . The ego agent with neighboring collaborators will collaboratively predict the bounding boxes  $\hat{Y} = f(\mathcal{X}(\mathcal{S}, \mathcal{I}); \tau)$  based on the aggregated sensing observations  $\mathcal{X}$ , where  $f$  is the V2X 3D detection model, and  $\tau$  is the fusion strategy including early, late and intermediate fusion.

Our objective is to attack the V2X perception model by adjusting initial normal scenes to be more challenging. There are two types of adversaries in this work, namely agent collaboration combination  $\mathcal{I}$  and pose perturbation  $\Delta$ . These two adversaries will modify the sensor viewpoint and vehicle poses in a physically plausible way and CARLA [36] is leveraged to simulate the updated observations  $\mathcal{X}(\mathcal{S} + \Delta, \mathcal{I})$ .

We then define the adversarial objective  $\mathcal{L}_{\text{adv}}$  (Section III-D) which is minimized to generate challenging scenes:

$$\begin{aligned} \Delta^*, \mathcal{I}^* = \arg \min_{\Delta, \mathcal{I}} \quad & \mathcal{L}_{\text{adv}}(f(\mathcal{X}(\mathcal{S} + \Delta, \mathcal{I}); \tau), Y) \\ \text{s.t.} \quad & \|\Delta\| \leq \delta, \mathcal{I} \subset \mathcal{A}, |\mathcal{I}| = k \end{aligned} \quad (2)$$

where  $|\cdot|$  is the set cardinality and  $Y$  is the ground truth bounding boxes. We decouple the above formula and optimize

this factorized approximation as follows:

$$\begin{aligned} \mathcal{I}^* = \arg \min_{\mathcal{I}} \quad & \mathcal{L}_{\text{adv}}(f(\mathcal{X}(\mathcal{S}, \mathcal{I}); \tau), Y) \\ \text{s.t.} \quad & \mathcal{I} \subset \mathcal{A}, |\mathcal{I}| = k \end{aligned} \quad (3)$$

$$\begin{aligned} \Delta^* = \arg \min_{\Delta} \quad & \mathcal{L}_{\text{adv}}(f(\mathcal{X}(\mathcal{S} + \Delta, \mathcal{I}^*); \tau), Y) \\ \text{s.t.} \quad & \|\Delta\| \leq \delta \end{aligned} \quad (4)$$

Such factorization can separate optimization into two subsequent tasks: adversarial collaborator search (Eq. 3) and adversarial pose perturbation (Eq. 4), which can not only simplify the optimization but also provides the possibility of analyzing two stages individually to better understand the performance of the target system. As the performance drop brought by pose perturbation can be easily diminished by changing sensor viewpoints, we choose to search collaboration first instead of the reverse order. For multi-agent systems,  $k = 1$  will clearly lead to inferior performance. However, we are interested in studying the robustness of V2X system even when it is deployed at scale. Thus we fix  $k = 3$  in this work.

### B. Adversarial Collaborator Search

Although examining all the agent combinations may seem appealing at first but it is prohibitively expensive due to the enormous combinations and the high computation cost. Thus instead, we design an efficient search algorithm. We adopt the intermediate fusion model AttFuse [42] to construct the collaboration graph where the learnable edge weights are considered to represent the importance of that agent's feature contribution to the ego agent. We leverage these learnable edge weights to define each agent's weakness level so that lower values represent smaller contributions to the overall perception system and thus, assigning these weak agents with higher sampling probability can increase the chance of finding adversarial collaborators with inferior performance. Although

other fusion methods such as Early Fusion and Late Fusion can't produce collaboration graphs with important weights, we experimentally demonstrate that the proposed attention-based probabilistic sampling method can be transferred to other models with great search efficiency (IV). In addition, our framework is general and other adversarial collaborator search methods can be integrated into the framework and we encourage more researchers to investigate this new direction.

To obtain the edge weights for all agents, we first equip all agents with LiDAR sensor in the simulator. Each agent will reason intermediate features based on its raw sensing observation and then transmit their intermediate features  $\mathbf{H}_i \in \mathbb{R}^{H \times W \times C}$  to the ego agent. Then the self-attention model is employed to capture the feature importance from different agents in the same spatial locations under ego coordinate. Formally, let  $\mathbf{h}_{mn}^i = [\mathbf{H}_i]_{mn} \in \mathbb{R}^C$  be the feature from agent  $i$  in location  $(m, n)$  and  $\mathbf{h}_{mn} = \{\mathbf{h}_{mn}^1, \dots, \mathbf{h}_{mn}^N\} \in \mathbb{R}^{N \times C}$  is the aggregated features for location  $(m, n)$  from all  $N$  agents. Then the attention is operated as follows:

$$\mathbf{a}_{mn} = \text{softmax} \left( \frac{\mathbf{q}_{mn} \mathbf{k}_{mn}^T}{\sqrt{C}} \right) \quad (5)$$

where  $\mathbf{q}_{mn}$ ,  $\mathbf{k}_{mn}$  and  $\mathbf{v}_{mn}$  are linear projections of  $\mathbf{h}_{mn}$  along channel dimension. The fused feature  $\mathbf{h}'_{mn} = \mathbf{a}_{mn} \mathbf{v}_{mn}$ . It can be sliced and rearranged to get the updated feature  $\mathbf{H}'_i$ .

Before applying this self-attention model in our scene generator, we will train it on the augmented OPV2V dataset [42] to learn the collaboration graph construction by sending  $\mathbf{H}'_i$  to a detection header to produce bounding box predictions. During the adversarial procedure, we fix the network's weights and directly exploit calculated  $\mathbf{a}_{mn}$  to detect the adversarial collaborators. As the attention weights are position-wise, average pooling is adopted to aggregate the weights of all spatial locations.

$$s_j = \text{Avg}([\mathbf{a}_{11}]_{i_*j}, \dots, [\mathbf{a}_{HW}]_{i_*j}) \quad (6)$$

Here  $s_j$  represents the importance of agent  $j$  and thus  $1/s_j$  is the associated weakness level for this agent. For each collaborator combination  $\mathcal{I}$ , we can model its weakness level as the sum of the individual agent's weakness level and apply softmax to form a probability distribution:

$$\mathbf{w} = \{w_{\mathcal{I}} = \sum_{i \in \mathcal{I}} \frac{1}{s_i} | \mathcal{I} \subset \mathcal{A}, |\mathcal{I}| = k\} \quad (7)$$

$$\mathbf{p} = \text{Softmax} \left( \frac{\mathbf{w}}{\tau} \right) \quad (8)$$

where  $\tau$  is the temperature parameter to control the shape of the distribution. We sample  $k_0$  combinations without replacement according to the probability  $\mathbf{p}$ , examine all the adversarial objective values, and keep the best one with the lowest adversarial value as the adversarial collaboration combination  $\mathcal{I}^*$ . This combination is eventually used to build the adversarial collaboration graph where only the selected agents can share the information with each other.

### C. Adversarial Perturbation Search

**Search space:** We perturb multiple agents' poses within physical plausible bounds. Each agent's perturbation is

---

### Algorithm 1 Adversarial perturbation search

---

- 1: Sample  $m$  agents to perturb according to heuristics
  - 2: Generate context-aware feasible set  $\mathcal{Q}$  for  $m$  agents
  - 3: Initialize historical observation  $\mathcal{D} = \{\}$
  - 4: **for**  $i = 1 \dots M$  **do**
  - 5:   Generate  $\Delta^{(i)}$  based on historical observation  $\mathcal{D}$  and black-box search algorithm
  - 6:   Project  $\Delta^{(i)}$  onto feasible set  $\mathcal{Q}$
  - 7:   Get updated sensing observation from LiDAR simulator  $\mathcal{X}^{(i)} = \mathcal{X}(\mathcal{S} + \Delta^{(i)}, \mathcal{I}^*)$
  - 8:    $\mathcal{L}_{\text{adv}}^{(i)} = \mathcal{L}_{\text{adv}}(f(\mathcal{X}^{(i)}), Y)$
  - 9:    $\mathcal{D} = \mathcal{D} \cup \{(\Delta^{(i)}, \mathcal{L}_{\text{adv}}^{(i)})\}$
  - 10: **end for**
  - 11:  $\Delta^{(*)} = \arg \min_{\Delta^{(i)}, i \in \{1, \dots, M\}} \mathcal{L}_{\text{adv}}^{(i)}$
- 

parameterized as  $\delta_i = (\delta x_i, \delta y_i, \delta \theta_i)$ , where  $(\delta x_i, \delta y_i)$  is the perturbation of the location and  $\delta \theta_i$  is the change of yaw angle. The multi-agent perturbation is then

$$\Delta = \{\delta_1, \delta_2, \dots, \delta_m\} \quad (9)$$

where  $m$  is the number of perturbed agents and these  $m$  agents are sampled according to an occlusion-inspired heuristic from the set  $\mathcal{A}$ . We rank  $N$  agents by occlusion levels in decreasing order and then select the top  $m$  agents to perturb. Specifically, each agent's occlusion level is the sum of its intrinsic-occlusion score and extrinsic-occlusion score. The intrinsic-occlusion score is 1 if the agent is partially overlapped by any other agent in the scene, indicating the occlusion level of the perturbed agent (occludee). The extrinsic-occlusion score measures how many other agents in the scene can be partially occluded by the examined agent (occluder). For the multi-agent V2X system, we sum the occlusion score from different viewpoints as the agent's overall score. In this way, the sampled agents are more likely to observe partially occluded objects. We set  $\|\Delta\| \leq \delta$  to constrain the perturbation within a limited range. In this work,  $m = 3$  is adopted for increased search space and scenario configurations.

**Black-box search algorithm:** Our framework is amenable to any black-box search algorithm. The search algorithm seeks to find challenging scenes for the V2X perception model by minimizing the adversarial objective  $\mathcal{L}_{\text{adv}}$ . In this paper, we benchmark 3 black-box search algorithms: Random Search (RS), Genetic Algorithm (GA) [60] and Bayesian Optimization (BO) [61]. The Random Search will randomly sample perturbation from the feasible set. The Genetic Algorithm will maintain a population of candidate perturbations, evolve the population over time by selecting parents with high fitness scores, and the best candidate is always kept for enhanced performance [60]. The Bayesian Optimization will build a surrogate model and use the acquisition function to balance the exploration and exploitation for generating candidates.

**Search pipeline:** The overall method is summarized in Algorithm 1. To increase the plausibility of the perturbation, we build a context-aware feasible perturbation set  $\mathcal{Q}$  for the sampled  $m$  agents. To generate such a feasible set, we first

uniformly sample  $N_Q = 1000$  potential perturbations within the bounds ( $\delta x, \delta y \in [-2.5, 2.5]$  m and  $\delta\theta \in [-45^\circ, 45^\circ]$ ) and remove the ones that can cause potential collisions. As the location and angle have different magnitudes, to diminish this bias, we also normalize the perturbation  $\Delta$  by dividing it by the perturbation range s.t.  $\|\Delta\|_\infty \leq 1$ . A historical observation  $\mathcal{D}$  of  $(\Delta, \mathcal{L}_{adv})$  pairs is maintained through the optimization process. During each iteration, the search algorithm generates the potential perturbation  $\Delta$  and projects it onto the feasible set  $\mathcal{Q}$  by finding the closest element in the set measured in  $\ell_2$  distance. Then it will query the target V2X perception model to obtain adversarial loss  $\mathcal{L}_{adv}$ . The search algorithm will update the historical observation  $\mathcal{D}$ , which is used to generate the perturbation for the next iteration. The best-observed perturbation with the lowest adversarial loss is selected for the final perturbation.

#### D. Adversarial Objective

We adopt weighted average precision as the adversarial loss.

$$\mathcal{L}_{adv} = \sum_{t \in \mathcal{T}} w_t \text{AP}@t \quad (10)$$

where  $\mathcal{T}$  is a set of Intersection of Union (IoU) thresholds and in our experiment,  $\mathcal{T} = \{0.3, 0.5, 0.7\}$ .  $\text{AP}@t$  is the average precision (AP) at IoU of threshold  $t$  and  $w_t$  is the associated weight. Using this weighted sum of average precision can lead to smoother score change, which eases the difficulty of optimization. In this work, we set  $w_{0.3} = 1$ ,  $w_{0.5} = 0.8$  and  $w_{0.7} = 0.5$  to give higher weights for lower IoU thresholds as their APs are generally harder to decrease.

### IV. EXPERIMENTS

#### A. Experiment Setup

**Dataset:** Experiments are conducted in CARLA [36] simulator. Two datasets are used in the experiment: 1) we augment the existing large-scale Vehicle-to-Vehicle (V2V) perception dataset, namely OPV2V, with infrastructure sensor data. The OPV2V’s training split is used to train modern V2X perception models until convergence. From the augmented OPV2V’s test split, we have 94 driving logs and each has 70 frames, covering 8 road areas. Due to the high computational cost of running the CARLA simulator and deep networks, We sample 331 *Normal* scenes from these collected scenarios, and the train/validation splits for evaluating V2XP-ASG are 219/112. The major experiments are conducted in train split and the validation split is only used for reporting the performance of the fine-tuned model. 2) Besides the above data, we build another heuristic-generated challenging dataset called *Heuristic* that has high traffic density with severe occlusions and sparse observations. This hold-out dataset includes 321 frames sampled from 14 driving logs. We first collect 14 driving logs for a total of 980 frames with dense traffic (20~30 vehicles per frame) in 4 CARLA towns. Then for each frame, we calculate the average number of LiDAR points within the bounding boxes, and we curate the raw data by only keeping the scene with an average number of points less than the threshold  $N_{thred} = 25$ . As this dataset is

TABLE I: Evaluation of V2X perception models on *Normal* and V2XP-ASG generated *Challenging* scenes. The number within parentheses is the AP drop compared with *Normal*.

Methods	Scenes Type	AP@0.3	AP@0.5	AP@0.7
No Fusion	Normal	55.4	54.8	46.3
	Challenging	31.1(-24.3)	30.3(-24.5)	25.1(-21.2)
Late Fusion	Normal	73.4	72.6	62.6
	Challenging	42.0(-31.4)	40.0(-32.6)	32.8(-29.8)
Early Fusion	Normal	80.3	79.8	73.5
	Challenging	49.8(-30.5)	48.3(-31.5)	43.4(-30.1)
AttFuse	Normal	82.4	81.5	74.6
	Challenging	46.6(-35.8)	44.9(-36.6)	40.5(-34.1)

only visible during inference, it provides a fairer evaluation of whether the fine-tuned model can achieve better results in unseen challenging scenes (Table II).

**V2X perception model:** V2XP-ASG is evaluated on 4 models: 1) No Fusion, which predicts bounding boxes only based on ego-agent LiDAR point clouds. 2) Late Fusion, where detection proposals of each agent are transmitted and the non-maximum suppression is applied to generate the final predictions. 3) Early Fusion, which aggregates raw LiDAR points from different agents to a holistic view and feeds them to the detector. 4) AttFuse [42], an intermediate fusion model which broadcasts intermediate features with each other and uses location-wise self-attention to fuse received features. All the models are implemented with PointPillar [62] backbone. **V2XP-ASG:** We adopt AttFuse’s attention weights for constructing the adversarial collaboration graph for all 3 V2X perception models. The temperature parameter  $\tau = 0.03$  and we examine  $k_0 = 3$  combinations sampled according to Eq. 8. For the main experiments, we adopt the Bayesian Optimization [61] as the black-box search algorithm. For LiDAR simulations, to diminish the influence of noise, we set the noise to be zero i.e., zero drop-off rate and zero noise level so that the perception performance is solely affected by the intrinsic scene configurations. The perception performance is evaluated in the range of  $x, y \in [-48, 48]$  m. For consistent ground truth, when perturbing agents, we ensure that the updated poses still stay within the evaluation range. Parameters of black-box optimization can be found in the supplementary videos.

#### B. Experimental results

**V2X perception model evaluations:** The evaluation results for different V2X perception models are shown in Table I. The results demonstrate that our V2XP-ASG can generate challenging scenes for both single-agent and V2X perception systems with an average of 28.7% drop of AP@0.7, showing that V2XP-ASG can efficiently identify challenging scenes for a wide range of models with different fusion strategies.

**Improvement with challenging scenes:** We now investigate if our generated challenging scenes can help improve the performance of the V2X perception system. We first fine-tune the original AttFuse model on train split of its generated challenging scenes and then test the model on the val split of *Normal* and *Challenging* scenes. For a fairer comparison, we

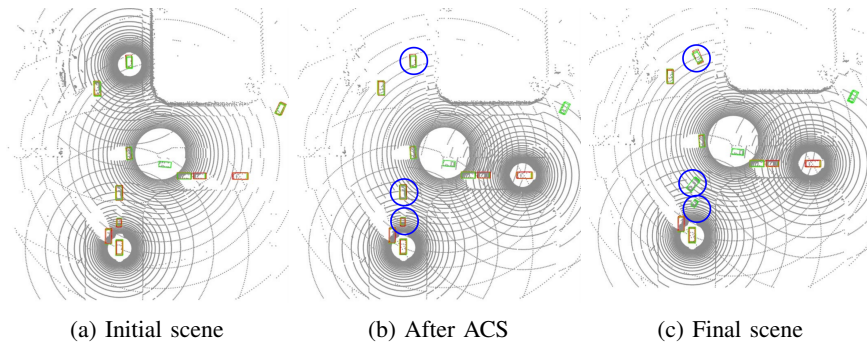


Fig. 2: Qualitative results of generated challenging scenes. (a) initial scene. (b) scene after selecting adversarial collaborators. (c) scene after vehicle pose perturbation. Blue circles represent the perturbed vehicles.

TABLE II: Improving AttFuse TABLE III: Transferability experiment in TABLE IV: Collaboration TABLE V: Compo- study. FT means fine-tuning on AP@0.7. The number in parentheses indi- selection method compari- nent ablation study train split of generated scenes cates the AP drop compared with *Normal*. son in AP@0.7. of ACS and APS.

Scene Types	Models	AP@0.7	Source				Target			ACS	APS	AP@0.7
			Late	Early	AttFuse	Normal	Late	Early	AttFuse			
Normal	AttFuse	70.6				Normal	62.6	73.5	74.2			74.6
	AttFuse+FT	<b>74.6</b>				ACS-R	56.1	66.7	70.1	✓		66.5
						ACS-A	<b>53.1</b>	<b>64.6</b>	<b>66.5</b>		✓	44.4
Heuristic	AttFuse	64.9										
	AttFuse+FT	<b>73.1</b>								✓	✓	<b>40.5</b>
Challenging	AttFuse	43.9										
	AttFuse+FT	<b>56.3</b>										

TABLE VI: Benchmark results of the black-box algorithms.

Methods	AP@0.3	AP@0.5	AP@0.7
Normal	82.4	81.5	74.6
Ransom Search (RS)	68.3	67.4	60.4
Genetic Algorithm (GA)	54.8	52.6	46.8
Bayesian Optimization (BO)	50.9	49.4	44.4

also evaluate its performance on a separate challenging hold-out set (*Heuristic*). As shown in Table II, the fine-tuned model show improvement for all 3 datasets, illustrating the great benefit of V2XP-ASG for improving perception systems.

**Transferability of challenging scenes:** Table III shows the transferability of V2XP-ASG generated scenes. The source model is used for generating challenging scenes and the target model is tested on these generated scenes. The performance is the best when testing the target model on the scenes generated by the same model. Moreover, three models all show great performance drop on each other’s generated challenging scenes than their performance on normal scenes, showing that the models have a certain degree of agreement on whether a scene is challenging and thus demonstrating the favored transferability of V2XP-ASG generated challenging scenes.

**Baseline comparison:** We compare the proposed AttFuse-based collaborator selection strategy (ACS-A) with random selection (ACS-R) that randomly sample  $k_0 = 3$  agent combinations. The experiment results are shown in Table IV. The proposed method can decrease the detection performance by 9.5%, 8.9%, 7.7% while random selection can only decrease the score by 6.5%, 6.8%, 4.1%, showing great efficiency of the proposed search strategy.

**Component analysis:** As shown in Table V, the proposed two components ACS and APS are both instrumental for find-

ing challenging scenes, demonstrating that both viewpoints and pose perturbation are critical for identifying challenging scenes for the multi-agent system.

**Black-box search benchmark results:** The benchmark results for different black-box search strategies are shown in Table VI. Both GA and BO outperform RS and BO reaches the best performance. We argue this is due to the good balance between exploration and exploitation of BO.

**Visualization results:** Figure 2 shows the visualization of V2XP-ASG generated *Challenging* scenes and the associated *Normal* scenes. As shown in Figure 2b, adversarial collaborator selection can change sensor viewpoint to make objects hard to detect. In Figure 2c, three agents are perturbed and two of the perturbed agents simultaneously take a right turn, which is realistic and rare in real world. It demonstrates that the V2XP-ASG generated scenes are both challenging and meaningful for testing the perception module.

## V. CONCLUSIONS

In this work, we present the first open adversarial scene generation framework dubbed V2XP-ASG for LiDAR-based V2X perception systems. The experiments demonstrate that the V2XP-ASG can create challenging scenes for a wide range of perception models, including single-agent and V2X perception systems. In particular, by training on generated scenes, the performance of the perception system can be further improved for both common and challenging scenes. Moreover, the ablation study verifies that the proposed attention-based probabilistic sampling approach can effectively find adversarial collaborators and the two novel components are both advantageous for generating challenging scenes.

## VI. ACKNOWLEDGEMENT

This work is part of the OpenCDA Ecosystem [63] and is supported by the Federal Highway Administration with Grant number 693JJ321C000016.

## REFERENCES

- [1] W. Liu, L. Xiong, X. Xia, Y. Lu, L. Gao, and S. Song, "Vision-aided intelligent vehicle sideslip angle estimation based on a dynamic model," *IET Intelligent Transport Systems*, vol. 14, no. 10, pp. 1183–1189, 2020.
- [2] W. Liu, L. Xiong, X. Xia, and Z. Yu, "Intelligent vehicle sideslip angle estimation considering measurement signals delay," in *2018 IEEE Intelligent Vehicles Symposium (IV)*. IEEE, 2018, pp. 1584–1589.
- [3] A. Pal, Y. Qiu, and H. Christensen, "Learning hierarchical relationships for object-goal navigation," in *Conference on Robot Learning*. PMLR, 2021, pp. 517–528.
- [4] Y. H. Khalil and H. T. Mouftah, "Licanet: Further enhancement of joint perception and motion prediction based on multi-modal fusion," *IEEE Open Journal of Intelligent Transportation Systems*, vol. 3, pp. 222–235, 2022.
- [5] S. Kitajima, H. Chouchane, J. Antona-Makoshi, N. Uchida, and J. Tajima, "A nationwide impact assessment of automated driving systems on traffic safety using multiagent traffic simulations," *IEEE Open Journal of Intelligent Transportation Systems*, vol. 3, pp. 302–312, 2022.
- [6] V. Papathanasopoulou, I. Spyropoulou, H. Perakis, V. Gikas, and E. Andrikopoulou, "A data-driven model for pedestrian behavior classification and trajectory prediction," *IEEE Open Journal of Intelligent Transportation Systems*, vol. 3, pp. 328–339, 2022.
- [7] J. Betz, H. Zheng, A. Liniger, U. Rosolia, P. Karle, M. Behl, V. Krovi, and R. Mangharam, "Autonomous vehicles on the edge: A survey on autonomous vehicle racing," *IEEE Open Journal of Intelligent Transportation Systems*, vol. 3, pp. 458–488, 2022.
- [8] A. Nayak, A. Eskandarian, and Z. Doerzaph, "Uncertainty estimation of pedestrian future trajectory using bayesian approximation," *IEEE Open Journal of Intelligent Transportation Systems*, vol. 3, pp. 617–630, 2022.
- [9] M. Masmoudi, H. Friji, H. Ghazzai, and Y. Massoud, "A reinforcement learning framework for video frame-based autonomous car-following," *IEEE Open Journal of Intelligent Transportation Systems*, vol. 2, pp. 111–127, 2021.
- [10] S. Mukherjee, A. M. Wallace, and S. Wang, "Predicting vehicle behavior using automotive radar and recurrent neural networks," *IEEE Open Journal of Intelligent Transportation Systems*, vol. 2, pp. 254–268, 2021.
- [11] H. Christensen, D. Paz, H. Zhang, D. Meyer, H. Xiang, Y. Han, Y. Liu, A. Liang, Z. Zhong, and S. Tang, "Autonomous vehicles for micro-mobility," *Autonomous Intelligent Systems*, vol. 1, pp. 1–35, 2021.
- [12] R. De Iaco, S. L. Smith, and K. Czarniecki, "Universally safe swerve maneuvers for autonomous driving," *IEEE Open Journal of Intelligent Transportation Systems*, vol. 2, pp. 482–494, 2021.
- [13] W. Liu, K. Quijano, and M. M. Crawford, "Yolov5-tassel: detecting tassels in rgb uav imagery with improved yolov5 based on transfer learning," *IEEE Journal of Selected Topics in Applied Earth Observations and Remote Sensing*, vol. 15, pp. 8085–8094, 2022.
- [14] Y. Han, Y. Liu, D. Paz, and H. Christensen, "Auto-calibration method using stop signs for urban autonomous driving applications," in *2021 IEEE International Conference on Robotics and Automation (ICRA)*. IEEE, 2021, pp. 13 179–13 185.
- [15] R. Xu, Y. Guo, X. Han, X. Xia, H. Xiang, and J. Ma, "Opencda: an open cooperative driving automation framework integrated with co-simulation," in *2021 IEEE International Intelligent Transportation Systems Conference (ITSC)*. IEEE, 2021, pp. 1155–1162.
- [16] G. Chen, X. Zhao, Z. Gao, and M. Hua, "Dynamic drifting control for general path tracking of autonomous vehicles," *IEEE Transactions on Intelligent Vehicles*, 2023.
- [17] M. Hua, G. Chen, B. Zhang, and Y. Huang, "A hierarchical energy efficiency optimization control strategy for distributed drive electric vehicles," *Proceedings of the Institution of Mechanical Engineers, Part D: Journal of Automobile Engineering*, vol. 233, no. 3, pp. 605–621, 2019.
- [18] H. Yu, Y. Luo, M. Shu, Y. Huo, Z. Yang, Y. Shi, Z. Guo, H. Li, X. Hu, J. Yuan *et al.*, "Dair-v2x: A large-scale dataset for vehicle-infrastructure cooperative 3d object detection," *arXiv preprint arXiv:2204.05575*, 2022.
- [19] Y. Yuan, H. Cheng, M. Y. Yang, and M. Sester, "Generating evidential bev maps in continuous driving space," *arXiv preprint arXiv:2302.02928*, 2023.
- [20] R. Valiente, B. Toghi, R. Pedarsani, and Y. P. Fallah, "Robustness and adaptability of reinforcement learning-based cooperative autonomous driving in mixed-autonomy traffic," *IEEE Open Journal of Intelligent Transportation Systems*, vol. 3, pp. 397–410, 2022.
- [21] Z. Ali, W. U. Khan, A. Ihsan, O. Waqar, G. A. S. Sidhu, and N. Kumar, "Optimizing resource allocation for 6g noma-enabled cooperative vehicular networks," *IEEE Open Journal of Intelligent Transportation Systems*, vol. 2, pp. 269–281, 2021.
- [22] Y. Yuan and M. Sester, "Comap: A synthetic dataset for collective multi-agent perception of autonomous driving," *The International Archives of the Photogrammetry, Remote Sensing and Spatial Information Sciences*, vol. XLIII-B2-2021, pp. 255–263, 2021.
- [23] H. Xie, Y. Wang, X. Su, S. Wang, and L. Wang, "Safe driving model based on v2v vehicle communication," *IEEE Open Journal of Intelligent Transportation Systems*, vol. 3, pp. 449–457, 2022.
- [24] R. Xu, H. Xiang, Z. Tu, X. Xia, M.-H. Yang, and J. Ma, "V2x-vit: Vehicle-to-everything cooperative perception with vision transformer," *arXiv preprint arXiv:2203.10638*, 2022.
- [25] Y. Hu, S. Fang, Z. Lei, Y. Zhong, and S. Chen, "Where2comm: Communication-efficient collaborative perception via spatial confidence maps," *arXiv preprint arXiv:2209.12836*, 2022.
- [26] Y. Li, D. Ma, Z. An, Z. Wang, Y. Zhong, S. Chen, and C. Feng, "V2x-sim: Multi-agent collaborative perception dataset and benchmark for autonomous driving," *IEEE Robotics and Automation Letters*, vol. 7, no. 4, pp. 10 914–10 921, 2022.
- [27] Y. Yuan and M. Sester, "Leveraging dynamic objects for relative localization correction in a connected autonomous vehicle network," *arXiv preprint arXiv:2205.09418*, 2022.
- [28] Z. Lei, S. Ren, Y. Hu, W. Zhang, and S. Chen, "Latency-aware collaborative perception," *arXiv preprint arXiv:2207.08560*, 2022.
- [29] S. Tan, K. Wong, S. Wang, S. Manivasagam, M. Ren, and R. Urtasun, "Scenegen: Learning to generate realistic traffic scenes," in *Proceedings of the IEEE/CVF Conference on Computer Vision and Pattern Recognition*, 2021, pp. 892–901.
- [30] S. Suo, S. Regalado, S. Casas, and R. Urtasun, "TrafficSim: Learning to simulate realistic multi-agent behaviors," in *Proceedings of the IEEE/CVF Conference on Computer Vision and Pattern Recognition*, 2021, pp. 10 400–10 409.
- [31] Y. Luo, P. Cai, Y. Lee, and D. Hsu, "Simulating autonomous driving in massive mixed urban traffic," *arXiv preprint arXiv:2011.05767*, 2020.
- [32] Y. Abeyirigoonawardena, F. Shkurti, and G. Dudek, "Generating adversarial driving scenarios in high-fidelity simulators," in *2019 International Conference on Robotics and Automation (ICRA)*. IEEE, 2019, pp. 8271–8277.
- [33] D. Rempe, J. Philion, L. J. Guibas, S. Fidler, and O. Litany, "Generating useful accident-prone driving scenarios via a learned traffic prior," in *Conference on Computer Vision and Pattern Recognition (CVPR)*, 2022.
- [34] J. Wang, A. Pun, J. Tu, S. Manivasagam, A. Sadat, S. Casas, M. Ren, and R. Urtasun, "AdvSim: Generating safety-critical scenarios for self-driving vehicles," in *Proceedings of the IEEE/CVF Conference on Computer Vision and Pattern Recognition*, 2021, pp. 9909–9918.
- [35] Y.-C. Liu, J. Tian, C.-Y. Ma, N. Glaser, C.-W. Kuo, and Z. Kira, "Who2com: Collaborative perception via learnable handshake communication," in *2020 IEEE International Conference on Robotics and Automation (ICRA)*. IEEE, 2020, pp. 6876–6883.
- [36] A. Dosovitskiy, G. Ros, F. Codevilla, A. Lopez, and V. Koltun, "Carla: An open urban driving simulator," in *Conference on robot learning*. PMLR, 2017, pp. 1–16.
- [37] Q. Chen, S. Tang, Q. Yang, and S. Fu, "Cooper: Cooperative perception for connected autonomous vehicles based on 3d point clouds," in *2019 IEEE 39th International Conference on Distributed Computing Systems (ICDCS)*. OPTorganization, 2019, pp. 514–524.
- [38] Z. Y. Rawashdeh and Z. Wang, "Collaborative automated driving: A machine learning-based method to enhance the accuracy of shared information," in *2018 21st International Conference on Intelligent Transportation Systems (ITSC)*. OPTorganization, 2018, pp. 3961–3966.

- [39] A. Rauch, F. Klanner, R. Rasshofer, and K. Dietmayer, "Car2x-based perception in a high-level fusion architecture for cooperative perception systems," in *2012 IEEE Intelligent Vehicles Symposium*. OPTOrganization, 2012, pp. 270–275.
- [40] R. Song, A. Hegde, N. Senel, A. Knoll, and A. Festag, "Edge-aided sensor data sharing in vehicular communication networks," in *2022 IEEE 95th Vehicular Technology Conference: (VTC2022-Spring)*, 2022, pp. 1–7.
- [41] T.-H. Wang, S. Manivasagam, M. Liang, B. Yang, W. Zeng, and R. Urtasun, "V2vnet: Vehicle-to-vehicle communication for joint perception and prediction." Springer, 2020, pp. 605–621.
- [42] R. Xu, H. Xiang, X. Xia, X. Han, J. Li, and J. Ma, "Opv2v: An open benchmark dataset and fusion pipeline for perception with vehicle-to-vehicle communication," in *2022 International Conference on Robotics and Automation (ICRA)*. IEEE, 2022, pp. 2583–2589.
- [43] Y. Yuan, H. Cheng, and M. Sester, "Keypoints-based deep feature fusion for cooperative vehicle detection of autonomous driving," *IEEE Robotics and Automation Letters*, 2022.
- [44] Y. Li, S. Ren, P. Wu, S. Chen, C. Feng, and W. Zhang, "Learning distilled collaboration graph for multi-agent perception," *Advances in Neural Information Processing Systems*, vol. 34, 2021.
- [45] D. Qiao and F. Zulkernine, "Adaptive feature fusion for cooperative perception using lidar point clouds," *arXiv preprint arXiv:2208.00116*, 2022.
- [46] R. Xu, Z. Tu, H. Xiang, W. Shao, B. Zhou, and J. Ma, "Cobevt: Cooperative bird's eye view semantic segmentation with sparse transformers," *arXiv preprint arXiv:2207.02202*, 2022.
- [47] J. Cui, H. Qiu, D. Chen, P. Stone, and Y. Zhu, "Coopernaut: End-to-end driving with cooperative perception for networked vehicles," *arXiv preprint arXiv:2205.02222*, 2022.
- [48] S. Su, Y. Li, S. He, S. Han, C. Feng, C. Ding, and F. Miao, "Uncertainty quantification of collaborative detection for self-driving," 2023.
- [49] R. Song, L. Zhou, V. Lakshminarasimhan, A. Festag, and A. Knoll, "Federated learning framework coping with hierarchical heterogeneity in cooperative its," *arXiv preprint arXiv:2204.00215*, 2022.
- [50] R. Song, D. Liu, D. Z. Chen, A. Festag, C. Trinitis, M. Schulz, and A. Knoll, "Federated learning via decentralized dataset distillation in resource-constrained edge environments," *arXiv preprint arXiv:2208.11311*, 2022.
- [51] G. Chen, F. Wang, W. Li, L. Hong, J. Conradt, J. Chen, Z. Zhang, Y. Lu, and A. Knoll, "Neuroiv: Neuromorphic vision meets intelligent vehicle towards safe driving with a new database and baseline evaluations," *IEEE Transactions on Intelligent Transportation Systems*, vol. 23, no. 2, pp. 1171–1183, 2022.
- [52] M. Klischat and M. Althoff, "Generating critical test scenarios for automated vehicles with evolutionary algorithms," in *2019 IEEE Intelligent Vehicles Symposium (IV)*. IEEE, 2019, pp. 2352–2358.
- [53] J. Norden, M. O'Kelly, and A. Sinha, "Efficient black-box assessment of autonomous vehicle safety," *arXiv preprint arXiv:1912.03618*, 2019.
- [54] M. O'Kelly, A. Sinha, H. Namkoong, R. Tedrake, and J. C. Duchi, "Scalable end-to-end autonomous vehicle testing via rare-event simulation," *Advances in neural information processing systems*, vol. 31, 2018.
- [55] J. Tu, M. Ren, S. Manivasagam, M. Liang, B. Yang, R. Du, F. Cheng, and R. Urtasun, "Physically realizable adversarial examples for lidar object detection," in *Proceedings of the IEEE/CVF Conference on Computer Vision and Pattern Recognition*, 2020, pp. 13 716–13 725.
- [56] Y. Li, C. Wen, F. Juefei-Xu, and C. Feng, "Fooling lidar perception via adversarial trajectory perturbation," in *Proceedings of the IEEE/CVF International Conference on Computer Vision*, 2021, pp. 7898–7907.
- [57] Y. Cao, C. Xiao, B. Cyr, Y. Zhou, W. Park, S. Rampazzi, Q. A. Chen, K. Fu, and Z. M. Mao, "Adversarial sensor attack on lidar-based perception in autonomous driving," in *Proceedings of the 2019 ACM SIGSAC conference on computer and communications security*, 2019, pp. 2267–2281.
- [58] J. Tu, T. Wang, J. Wang, S. Manivasagam, M. Ren, and R. Urtasun, "Adversarial attacks on multi-agent communication," in *Proceedings of the IEEE/CVF International Conference on Computer Vision*, 2021, pp. 7768–7777.
- [59] Y.-C. Liu, J. Tian, N. Glaser, and Z. Kira, "When2com: Multi-agent perception via communication graph grouping," in *Proceedings of the IEEE/CVF Conference on computer vision and pattern recognition*, 2020, pp. 4106–4115.
- [60] M. Alzantot, Y. Sharma, S. Chakraborty, H. Zhang, C.-J. Hsieh, and M. B. Srivastava, "Genattack: Practical black-box attacks with gradient-free optimization," in *Proceedings of the Genetic and Evolutionary Computation Conference*, 2019, pp. 1111–1119.
- [61] B. Ru, A. Cobb, A. Blaas, and Y. Gal, "Bayesopt adversarial attack," in *International Conference on Learning Representations*, 2019.
- [62] A. H. Lang, S. Vora, H. Caesar, L. Zhou, J. Yang, and O. Beijbom, "Pointpillars: Fast encoders for object detection from point clouds," in *Proceedings of the IEEE/CVF Conference on Computer Vision and Pattern Recognition*, 2019, pp. 12 697–12 705.
- [63] R. Xu, H. Xiang, X. Han, X. Xia, Z. Meng, C.-J. Chen, C. Corrae-Jullian, and J. Ma, "The opencda open-source ecosystem for cooperative driving automation research," *IEEE Transactions on Intelligent Vehicles*, pp. 1–13, 2023.

# V2XP-ASG: Generating Adversarial Scenes for Vehicle-to-Everything Perception (Supplementary)

**Abstract**—In this supplementary, we first provide additional details for Adversarial Collaborator Search (ACS) including AttFuse model architecture (Sec. I-A), attention-based sampling approach (Sec. I-B) and ACS time complexity analysis (Sec. I-C). In the next section, we provide more technical details for Adversarial Perturbation Search. The selection criteria of agents to perturb is shown in Sec. II-A. Afterwords, we detail the feasible-set construction procedures (Sec. II-B). Then, we show the parameters and benchmark results for the implemented black-box optimization algorithms (Sec. II-C). In Sec. III, we provide additional information for experiment setup and the rule-based Heuristic dataset. In the end, we provide more visualizations for generated challenging scenes (Sec. IV-A) and qualitative results for improving AttFuse experiment (Sec. IV-B).

## I. ADVERSARIAL COLLABORATOR SEARCH

We assume each agent in the scene can independently simulate LiDAR observations. To achieve this, we conduct experiments in CARLA and mount LiDAR sensors for every agent in the scene. In this way, we can easily simulate LiDAR observations for selected intelligent agents with various LiDAR viewpoints, which are subsequently fed into V2X perception system to get the adversarial objective. Though verified in simulation, the proposed framework is general and can be easily adapted to other real-world experiments with high-fidelity realistic LiDAR simulators [?], [?] as demonstrated by previous work [?]. We first leverage the pre-trained AttFuse [?] to calculate the attention weights for all the agent pairs and then use the proposed attention-based sampling approach to efficiently search the adversarial collaborator combination. Notice that the AttFuse is pre-trained beforehand and stays fixed during the ACS process.

### A. AttFuse model architecture

**Metadata sharing and feature extraction:** Before, feature extraction, all the agents  $\mathcal{A}$  in the scene first share the metadata (e.g., poses and velocities, etc.) with each other and one of them is selected or specified as the ego agent which has a fixed pose during the whole scene generation process. After receiving this metadata, each agent projects its LiDAR observation to the ego-agent coordinate frame according to the relative pose and leverages PointPillar [?] backbones to extract intermediate features. More concretely, the projected LiDAR points are converted to a 2D pseudo-image filled with scattered pillar tensors and then the PointPillar backbone extracts the visual features  $\mathbf{H}_i \in \mathbb{R}^{H \times W \times C}$  for agent  $i$  with height  $H$ , width  $W$  and channel  $C$ .

**Compression and sharing:** These visual features are then compressed via  $1 \times 1$  convolutions along the channel dimension and then shared with all the agents in the scene.

Afterwords, the ego agent aggregates all the received features and applies  $1 \times 1$  deconvolutions to produce decompressed features  $\mathbf{H}_i \in \mathbb{R}^{H \times W \times C}$  with the original dimension.

**Attentive Fusion:** Now in the ego-agent side, we have formed a fully connected V2X collaboration graph where the nodes are agents' features. To fuse the features, self-attention is adopted. As LiDAR observations in different locations from the same agent usually have diverse qualities, thus instead of assigning scalar weights for attention scores, attention is operated in a location-wise manner. Formally, let  $\mathbf{h}_{mn}^i = [\mathbf{H}_i]_{mn} \in \mathbb{R}^C$ , denoting the agent  $i$ 's feature for location  $(m, n)$ . Then  $\mathbf{h}_{mn} = \{\mathbf{h}_{mn}^1, \dots, \mathbf{h}_{mn}^N\} \in \mathbb{R}^{N \times C}$  is the set of features for all  $N$  agents in the scene and attention is calculated as follows:

$$\mathbf{a}_{mn} = \text{softmax} \left( \frac{\mathbf{q}_{mn} \mathbf{k}_{mn}^T}{\sqrt{C}} \right) \quad (1)$$

$$\mathbf{h}'_{mn} = \mathbf{a}_{mn} \mathbf{v}_{mn} \quad (2)$$

where  $\mathbf{a} \in \mathbb{R}^{N \times N}$  is the attention weight and  $\mathbf{q}_{mn}, \mathbf{k}_{mn}, \mathbf{v}_{mn} \in \mathbb{R}^{N \times C}$  are linear projections of  $\mathbf{h}_{mn}$  along channel dimension. The fused feature  $\mathbf{h}'_{mn} \in \mathbb{R}^{N \times C}$  can be sliced and rearranged to get the updated intermediate feature  $\mathbf{H}'_i \in \mathbb{R}^{H \times W \times C}$  for agent  $i$ :

$$[\mathbf{H}'_i]_{mn} = [\mathbf{h}'_{mn}]_i \quad (3)$$

**Detection header:** The fused features are then passed through the detection and classification branch to generate the final bounding box predictions, which are used to define the detection training loss. This head is only used for pre-training the AttFuse and is ignored during the ACS process for computation efficiency.

**Detection loss:** The smooth  $\ell_1$  loss [?] is used for regression and the focal loss [?] is applied for learning the classification.

### B. Attention-based sampling approach

Training AttFuse beforehand can help learn to construct the collaboration graph which can be leveraged to associate each collaborator with an importance weight. We adopt pre-trained AttFuse for calculating the attention weights and argue different models have a certain degree of agreement on whether a collaborator is important or not, thus leveraging well-trained AttFuse can also help discover other models' adversarial collaborators. This argument is experimentally proved in Table 4. As the attention weights are position-wise, average pooling is adopted to aggregate the weights across different spatial locations.

$$s_j = \text{Avg}([\mathbf{a}_{11}]_{i_*j}, \dots, [\mathbf{a}_{HW}]_{i_*j}) \quad (4)$$

where  $i_*$  is the ego agent and  $s_j$  represents the importance of agent  $j$  and thus  $1/s_j$  is the associated weakness level for this agent. For each collaborator combination  $\mathcal{I}$ , its weakness level is characterized by the sum of the individual agent’s weakness level, which is further processed by softmax to form a probability distribution:

$$w_i = \frac{1}{s_i} \quad (5)$$

$$\mathbf{w} = \{w_{\mathcal{I}} = \sum_{i \in \mathcal{I}} w_i | \mathcal{I} \subset \mathcal{A}, |\mathcal{I}| = k\} \quad (6)$$

$$\mathbf{p} = \text{Softmax} \left( \frac{\mathbf{w}}{\tau} \right) \quad (7)$$

The temperature parameter  $\tau$  controls the shape of distribution and balances exploration and exploitation. Now we have formed a distribution over all possible collaborator combinations  $\{\mathcal{I} | \mathcal{I} \subset \mathcal{A}, |\mathcal{I}| = k\}$  and we can sample  $k_0$  combinations according to  $\mathcal{I} \sim \mathbf{p}$ . Each combination represents a set of intelligent agents that can sense the current scene from their own viewpoints. For each combination  $\mathcal{I}$ , we simulate these intelligent agents’ LiDAR observation and feed these observations to the target V2X perception model to calculate the adversarial objective  $\mathcal{L}_{\text{adv}}^{\mathcal{I}}$ . As a result, after examining  $k_0$  such combinations, we have formed a set of combination and loss pairs  $\{(\mathcal{I}_1, \mathcal{L}_{\text{adv}}^{\mathcal{I}_1}), \dots, (\mathcal{I}_{k_0}, \mathcal{L}_{\text{adv}}^{\mathcal{I}_{k_0}})\}$ . We choose the combination with the minimum loss as the final adversarial collaborator combination  $\mathcal{I}^*$  and build the adversarial collaboration graph with the set of selected agents in  $\mathcal{I}^*$  where each agent in this graph is an intelligent agent that can simulate LiDAR observation and communicate with other intelligent agents. This agent choice is then fixed for downstream adversarial pose perturbation.

### C. Time complexity

The main computation overhead in the ACS is the LiDAR simulation and running deep network. Accordingly, we focus on analyzing procedures involving such computation overhead. We first pass through the AttFuse network once to calculate the weights for all  $N$  agents. As we only need to calculate the attention for edges connected to ego agent and the computation can be done in parallel in multiple GPUs, thus the time complexity is  $\mathcal{O}(1)$ . Next, we examine  $k_0$  combinations and for each combination, we need to run LiDAR simulation and deep network once. Thus, the overall complexity is  $\mathcal{O}(k_0)$  ( $k_0 = 3$  in this work) while for brute force approach the time complexity is  $\mathcal{O}(C_N^k)$ . Take  $N = 20, k = 5$  as an example, the naive complexity is  $\mathcal{O}(C_{20}^5) = \mathcal{O}(15504)$  while our approach only needs  $\mathcal{O}(3)$ , showing the great computation efficiency of the proposed approach. Based on CARLA simulator and the examined perception models in this work, typically, the time for running LiDAR simulation and perception network once is around 100 ms. Therefore, for processing the previous example scene, the brute force approach requires around 25.8 min while the proposed approach only requires around 300 ms, showing the great computation benefits of the proposed approach.

TABLE I: Benchmark results of black-box optimization algorithm. Only adversarial pose perturbation is conducted for fair comparison.

Methods	AP@0.3	AP@0.5	AP@0.7
Normal	82.4	81.5	74.6
Ransom Search	68.3	67.4	60.4
Genetic Algorithm	54.8	52.6	46.8
Bayesian Optimization	50.9	49.4	44.4

## II. ADVERSARIAL PERTURBATION SEARCH

### A. Choosing agents to perturb

We leverage an occlusion-based heuristic to select agents to perturb. We rank  $N$  agents by occlusion levels in decreasing order and then select the top  $m$  agents to perturb. More specifically, for each agent, its occlusion level is the sum of its intrinsic-occlusion score and extrinsic-occlusion score. The intrinsic-occlusion score is 1 if the agent is partially overlapped by any other agent in the scene, indicating the occlusion level of the perturbed agent itself (occludee). Otherwise, the agent’s intrinsic-occlusion score is 0. Similarly, the extrinsic-occlusion score measures how many other agents in the scene can be occluded by the examined agent (occluder). We argue that perturbing agents with higher occlusion scores is more likely to make the scene more challenging as it has a higher chance of making either perturbed agents or neighboring agents (partially) occluded. For the V2X system, it involves multiple intelligent agents with distinct LiDAR viewpoints and for each viewpoint, we have a different set of occluder and occludee relationships, leading to different occlusion scores for each viewpoint. To this end, we sum each agent’s occlusion scores from different viewpoints as the overall occlusion score for this agent.

### B. Context-aware Feasible Set construction

To ensure that the perturbed pose is still realistic, perturbation is sampled only from a small range with feasibility constraints. In this work, we set  $\delta x \in [-2.5, 2.5]$  m,  $\delta y \in [-2.5, 2.5]$  m, and  $\delta \theta \in [-45^\circ, 45^\circ]$  as the boundary for perturbation where  $(\delta x, \delta y)$  is the location perturbation and  $\delta \theta$  is the yaw angle change. To construct the context-aware feasible set, we first uniformly sample  $N_Q = 1000$  multi-agent perturbations from the defined boundary and then prune infeasible ones by doing collision check and range check. Perturbations that can cause a collision with any agent in the scene will be removed from the set. The collision detection is done by checking the overlap of two vehicles’ 3D bounding boxes. If the overlap is greater than 0, then a collision exists between these two vehicles otherwise there is no collision. Moreover, we prune perturbations that lead to poses outside of the evaluation range. As the location and angle have different magnitudes, to diminish this bias, we also normalize the perturbation  $\Delta$  by dividing it by the range of pose perturbation s.t.

$$\|\Delta\|_\infty \leq 1 \quad (8)$$

### C. Blackbox Optimization

**Bayesian Optimization:** Bayesian optimization builds a surrogate model to probabilistically estimate the objective function and then search efficiently by using the acquisition function which can balance exploration and exploitation. In this work, Gaussian Process with Matern kernel ( $\nu = 2.5$ ) is selected for building the surrogate model. For the acquisition function, we adopt Upper Confidence Bound with  $\kappa = 2.5$  and  $\xi = 0$ . The number of samples for initializing BO is 20 and the BO iteration number is 30, leading to a total of 50 queries. The implementation is based on `bayes_opt` [?] package.

TABLE II: Hyperparameters for Genetic Algorithm.

Algorithm	Hyperparameters	Range/Value
Algo-	Max number of plateaus	5
	$z_0$	[-1,1]
Genetic	$z_{min}$	[-0.3,0.3]
	$p_0$	0.5
Algo-	$p_{min}$	0.1
	$\tau_{ga}$	0.8
gorithm	$\gamma$	0.9

maintains a population of candidate ( $\mathcal{P}$ ) perturbations and evolves the population by selecting the parents with high fitness values to produce child candidates. The fitness score  $\mathcal{F}$  and the selection probability  $\mathcal{P}_s$  are defined by using adversarial objectives, encouraging the algorithm to select parents with low adversarial objectives. More formally, they are defined as follows:

$$\mathcal{F} = \frac{1}{\mathcal{L}_{adv}^{\mathcal{P}}} \quad (9)$$

$$\mathcal{P}_s = \text{Softmax} \left( \frac{\mathcal{F}}{\tau_{ga}} \right) \quad (10)$$

where  $\mathcal{L}_{adv}^{\mathcal{P}}$  is the set of adversarial objectives of parents and  $\tau_{ga}$  controls the shape of the selection probability. Following [?], adaptive parameter scaling [?] is performed for better search performance:

$$p = \max(p_{min}, p_0 * \gamma^{\text{num\_plateaus}}) \quad (11)$$

$$z = \max(z_{min}, z_0 * \gamma^{\text{num\_plateaus}}) \quad (12)$$

where  $p$  is the mutation rate,  $z$  is the mutation range and  $\gamma$  is the hyperparameter to control the decay rate. The  $p_0$  and  $z_0$  are the initial mutation rate and mutation range respectively. The  $p_{min}$  and  $z_{min}$  are the minimum value of  $p$  and  $z$ . The `num_plateaus` is the number of times that the elite member of the child population is not better than the one of the parent population. The number of iterations is 6 and the population size is 10 for a total of 60 queries. The hyperparameters are detailed in Table II

**Random Search:** Random Search randomly samples a perturbation  $\Delta$  from the feasible set  $\mathcal{Q}$  and keeps track of the best perturbation so far through the iterations. The number of iterations is 100.

**Benchmark results:** The benchmark results for different black-box search strategies are shown in Table I. Both Genetic Algorithm and Bayesian optimization outperform

Random Search and the Bayesian Optimization reaches the best performance. We argue this is due to the good balance between exploration and exploitation of Bayesian Optimization, enabling efficient search.

### III. EXPERIMENT DETAILS

**Sensor Configuration:** Every intelligent agent is equipped with a 32-channel LiDAR. The LiDAR’s lower field of view (fov) is  $-25^\circ$  and the upper fov is  $2^\circ$ . The rotation frequency is 20 Hz and the points per second is 250000. Even in the same scene, LiDAR observations vary for different measurements because of the noise. As a result, the performance change induced by agent pose change can be actually caused by noises, hindering the adversarial search as we don’t just want to find a more noisy scene. To diminish the influence of noise, we set the noise to be zero i.e., zero drop-off rate and zero noise level. In this work, we focus on the case that the perception performance is solely affected by the intrinsic scene configurations.

**Ground truth:** The perception performance is evaluated in the range of  $x, y \in [-48, 48]$  m of the ego agent. The ego agent can be either an intelligent vehicle or infrastructure and its pose won’t change through the adversarial scene generation process. To ensure consistent ground truth, when perturbing agents, we ensure that the updated poses still stay within the evaluation range.

**Intelligent agent and perturbed agent selection:** We only consider agents within the evaluation range as potential intelligent agents. Moreover, agents to perturb are also ensured to be within the evaluation range.

**Heuristic holdout dataset:** For a fairer evaluation of the performance gain of leveraging challenging scenes generated by V2XP-ASG, we use heuristics to build a holdout challenging dataset dubbed *Heuristic*. We first collect 14 driving logs for a total of 980 frames with dense traffic (20~30 vehicles per frame) in 4 CARLA towns. Then for each frame, we calculate the average number of LiDAR points within the bounding boxes and we curate the raw data by only keeping the scene with an average number of points less than the threshold  $N_{thred} = 25$ . Eventually, we have 321 scenes as the *Heuristic* holdout dataset. This dataset is only used in Table 2 of the main paper. As this dataset is only visible during inference, it provides a fairer evaluation of whether the fine-tuned model can achieve better results in unseen/undiscovered challenging scenes.

### IV. MORE QUALITATIVE RESULTS

#### A. Challenging scene visualization:

More qualitative results for challenging scenes generated by V2XP-ASG are shown in Figure 1. From the figure, we can see that V2XP-ASG can efficiently identify challenging scenes for all 3 V2X perception models with 3 different fusion strategies. Notice that the figures of late fusion are Vehicle-to-Vehicle collaborations while the other 3 models’ figures are Vehicle-to-Infrastructure collaborations, demonstrating that the proposed V2XP-ASG can produce challenging scenes for V2X collaborations.

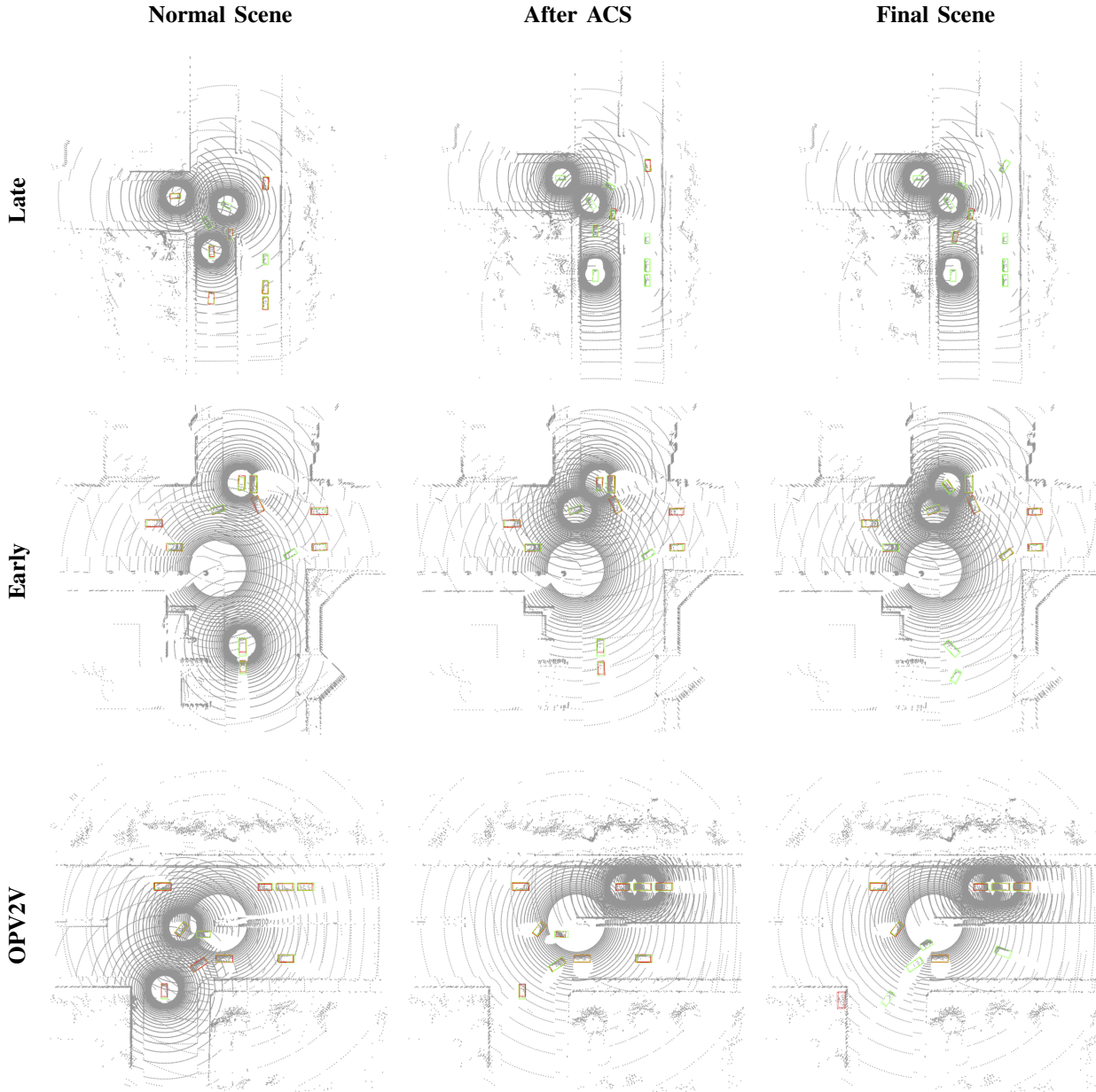
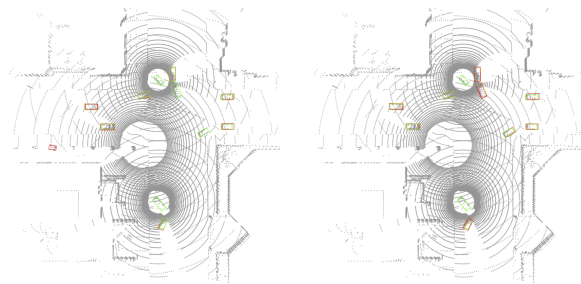


Fig. 1: Qualitative results of generated challenging scenes for V2X perception models. **Normal Scene:** The initial normal scenes. **After ACS:** The intermediate challenging scenes after Adversarial Collaborator Search (ACS). **Final Scene:** The final challenging scenes generated by V2XP-ASG with both Adversarial Collaborator Search (ACS) and Adversarial Perturbation search (APS).

### B. Improved AttFuse visualization:

In Figure 2, we plot the detection results for original AttFuse and fine-tuned AttFuse. The demonstrated scene is from the validation split of challenging scenes generated by V2XP-ASG and is not visible when fine-tuning AttFuse. From the figure, we can observe that the fine-tuned model can correctly identify more vehicles than the original one, illustrating that by leveraging the produced challenging scenes, we can further improve the model and achieve better results on the challenging scenes.



(a) Original AttFuse

(b) Fine-tuned AttFuse

Fig. 2: Qualitative results of original AttFuse [?] and fine-tuned AttFuse for the same challenging scene. The challenging scene is from the val split of challenging scenes produced by V2XP-ASG.